Heavy quark and quarkonium production at CERN LEP2: k_T-factorization versus data

A.V. Lipatov[a], N.P. Zotov

D.V. Skobeltsyn Institute of Nuclear Physics, M.V. Lomonosov Moscow State University, 119992 Moscow, Russia

Abstract. We present calculations of heavy quark and quarkonium production at CERN LEP2 in the k_T-factorization QCD approach. Both direct and resolved photon contributions are taken into account. A conservative error analysis is performed. The unintegrated gluon distribution in the photon is obtained from the full CCFM evolution equation. The traditional color-singlet mechanism to describe the non-perturbative transition of a $Q\bar{Q}$-pair into a final quarkonium is used. Our analysis covers the polarization properties of heavy quarkonia at moderate and large transverse momenta. We find that the total and differential open charm production cross sections are consistent with the recent experimental data taken by the L3, OPAL and ALEPH collaborations. At the same time the DELPHI data for the inclusive J/ψ production exceed our predictions, but experimental uncertainties are too large to claim a significant inconsistency. The bottom production in photon–photon collisions at CERN LEP2 is hard to explain within the k_T-factorization formalism.

1 Introduction

Heavy quark and quarkonium production in photon–photon collisions at high energies is a subject of intensive studies from both theoretical and experimental points of view [1–6]. From the theoretical side, heavy quarks in $\gamma\gamma$ collisions can be produced via the direct and resolved production mechanisms. In direct events, the two photons couple directly to a heavy quark pair. In resolved events, one photon ("single-resolved") or both photons ("double-resolved") fluctuate into a hadronic state, and a gluon or a quark of this hadronic fluctuation takes part in the hard interaction. At LEP2 conditions the contribution of the double-resolved events $(gg \to Q\bar{Q})$ is small [7], and charm and bottom quarks are produced mainly via direct $(\gamma\gamma \to Q\bar{Q})$ and single-resolved $(\gamma g \to Q\bar{Q})$ processes. The direct contribution is not dependent on the quark and gluon content in the photon, whereas the single-resolved processes strongly depend on the photon's gluon density. Therefore detailed knowledge of the gluon distributions in the photon is necessary for the theoretical description of such processes at modern (LEP2) and future (TESLA) colliders.

Usually quark and gluon densities are described by the Dokshitzer–Gribov–Lipatov–Altarelli–Parisi (DGLAP) evolution equation [8], where large logarithmic terms proportional to $\ln(\mu^2)$ are taken into account. The cross sections can be rewritten in terms of process-dependent hard matrix elements convoluted with quark or gluon density functions. In this way the dominant contributions come from diagrams where parton emissions in initial state are strongly ordered in virtuality. This is called collinear factorization, as the strong ordering means that the virtuality of the parton entering the hard scattering matrix elements can be neglected compared to the large scale μ^2. However, at high energies this hard scale is large compared to the Λ_{QCD} parameter, but on the other hand μ^2 is much smaller than the total energy $\sqrt{s}$ (around 200 GeV for the LEP2 collider). Therefore in such a case it was expected that the DGLAP evolution, which is only valid at large μ^2, should break down. The situation is classified as "semihard" [9–12].

It is believed that at asymptotically large energies (or small $x \sim \mu^2/s$) the theoretically correct description is given by the Balitsky–Fadin–Kuraev–Lipatov (BFKL) evolution equation [13] because here large terms proportional to $\ln(1/x)$ are taken into account. Just as for DGLAP, in this way it is possible to factorize an observable into a convolution of process-dependent hard matrix elements with universal gluon distributions. But as the virtualities (and transverse momenta) of the propagating gluons are no longer ordered, the matrix elements have to be taken off-shell and the convolution made also over transverse momentum $\mathbf{k}_T$ with the unintegrated (k_T-dependent) gluon distribution $\mathcal{F}(x, \mathbf{k}_T^2)$. The unintegrated gluon distribution $\mathcal{F}(x, \mathbf{k}_T^2)$ determines the probability to find a gluon carrying the longitudinal momentum fraction x and the transverse momentum $\mathbf{k}_T$. This generalized factorization is called k_T-factorization [10, 11].

The unintegrated gluon distribution is subject of intensive studies [14]. Various approaches to investigate this quantity have been proposed. One such approach, valid for

---

[a] e-mail: artem.lipatov@mail.ru

both small and large x, have been developed by Ciafaloni, Catani, Fiorani and Marchesini and is known as the CCFM model [15]. It introduces an angular ordering of emissions to correctly treat gluon coherence effects. In the limit of asymptotic energies, it is almost equivalent to BFKL [16–18], but also similar to the DGLAP evolution for large x and high μ^2. The resulting unintegrated gluon distribution depends on two scales; the additional scale $\bar{q}^2$ is a variable related to the maximum angle allowed in the emission and plays the role of the evolution scale μ^2 in the collinear parton densities. We will use the following classification scheme [14]: $\mathcal{F}(x, \mathbf{k}_T^2)$ is used for pure BFKL-type unintegrated gluon distributions and $\mathcal{A}(x, \mathbf{k}_T^2, \mu^2)$ stands for any other type having two scales involved.

The CCFM evolution equation formulated for the proton has been solved numerically or analytically in different ways [19–21]. As was shown [22–25], the unintegrated gluon distribution in the photon $\mathcal{A}_\gamma(x, \mathbf{k}_T^2, \mu^2)$ can be constructed by a method similar as in the proton[1]. But the situation is a bit different due to the pointlike component which reflects the splitting of the photon into a quark–antiquark pair. Also in the photon there are no sum rules equivalent to those in the proton case that constrain the quark distributions. However, this difference is not significant because the CCFM equation contains only gluon splitting, $g \to gg$. For the first time the unintegrated gluon density in the photon was obtained in [22] using a simplified solution of the CCFM equation in the single loop approximation, when small-x effects can be neglected. It means that the CCFM evolution is reduced to the DGLAP one with the difference that the single loop evolution takes the gluon transverse momentum k_T into account. Another simplified solution of the CCFM equation for a photon was proposed [23] using the Kimber–Martin–Ryskin (KMR) prescription [20]. In this way the μ^2-dependence in the unintegrated gluon distribution enters only in the last step of the evolution, and one-scale evolution equations can be used up to the last step. Both these methods give similar results [23]. The phenomenological unintegrated gluon density, based on the Golec-Biernat and Wüsthoff (GBW) saturation model [24] (extended to the large-x region), was proposed also [23]. Very recently the unintegrated gluon distribution in the photon $\mathcal{A}_\gamma(x, \mathbf{k}_T^2, \mu^2)$ was obtained [25] using the full CCFM evolution equation for the first time. It was shown that the full CCFM-evolved effective (integrated over $\mathbf{k}_T^2$) distribution is much higher than the usual DGLAP-based gluon density at $x < 10^{-1}$ region.

In the previous studies [23, 25] the unintegrated gluon distributions in a photon (obtained from the single loop as well as full CCFM evolution equation) were applied to the calculation of the open charm and bottom production at LEP2. It was found that the total cross section of the charm production is consistent with the experimental data. In contrast, the theoretical predictions of the bottom total cross section underestimate the data by a factor 2 or 3. But we note that all these calculations deal with

the total cross sections of the open charm and bottom production only. In this paper we will study heavy flavor production at LEP2 in more detail using the full CCFM-evolved unintegrated gluon density [25]. We will investigate the total and differential heavy quark cross section (namely pseudo-rapidity and transverse momenta distributions of the D^*-meson) and compare our theoretical results with the recent experimental data taken by the L3, OPAL and ALEPH collaborations at LEP2 [1–5].

Also we will study here the very intriguing problem connected with the inclusive J/ψ meson production at high energies. It traces back to the early 1990s, when the CDF data on the J/ψ and Υ hadroproduction cross section revealed a more than order of magnitude discrepancy with the theoretical expectations. This fact has resulted in intensive theoretical investigations of such processes. In the so-called non-relativistic QCD (NRQCD) [28] there are additional (octet) transition mechanism from the $c\bar{c}$-pair to the J/ψ mesons, where a $c\bar{c}$-pair is produced in the color octet (CO) state and transforms into a final color-singlet state (CS) with the help of soft gluon radiation. The CO model describes well the heavy quarkonium production at the Tevatron [29], although there are also some indications that it does not work well. For example, contributions from the octet mechanism to the J/ψ photo- and leptoproduction processes at HERA do not well reproduce [30] the experimental data. Also NRQCD does not predict J/ψ polarization properties at HERA and Tevatron [30,31]. At the same time the usual CS model supplemented with the k_T-factorization formalism gives a fully correct description of the inclusive J/ψ production at HERA [32] and Tevatron [33] including spin alignment of the quarkonium. The CO contributions within the k_T-factorization approach also will not contradict the experimental data if the parameters of the non-perturbative matrix elements will be reduced [33,34]. But this fact changes the hierarchy of these matrix elements which are obtained within the NRQCD.

Recently the DELPHI collaboration has presented experimental data [35] on the inclusive J/ψ production in $\gamma\gamma$ collisions at LEP2, which wait to be confronted with different theoretical predictions. The theoretical calculations [36] within the NRQCD formalism agree well with the DELPHI data. In contrast, the collinear DGLAP-based leading order perturbative QCD calculations in the CS model significantly (by order of magnitude) underestimate [36] the data. The aim of this paper, in particular, is to investigate whether the inclusive J/ψ production at LEP2 can be explained in the traditional CS model by using k_T-factorization and a CCFM-based unintegrated gluon density in the photon.

The outline of this paper is the following. In Sect. 2 we present the basic formalism of the k_T-factorization approach with a brief review of the calculation steps. In Sect. 3 we present the numerical results of our calculations. Finally, in Sect. 4, we give some conclusions. The compact analytic expressions for the off-shell matrix elements of all the subprocesses under consideration are given in the appendix. These formulas may be useful for the subsequent applications.

---

[1] See also [26], where we have used for the unintegrated gluon density in a photon the prescription proposed by Blümlein [27].

2 Cross sections for heavy flavor production

In $\gamma\gamma$ collisions heavy quark and quarkonium can be produced by one of the three mechanisms: direct production, single-resolved and double-resolved production processes. The direct contribution is governed by simple QED amplitudes which are independent on the gluon density in the photon. The double-resolved process gives a much smaller contribution than the direct and single-resolved processes [7] and will not be taken into account in this analysis.

Let $p_\gamma^{(1)}$ and $p_\gamma^{(2)}$ be the momenta of the incoming photons and p_1 and p_2 the momenta of the produced quarks. The single-resolved contribution to the $\gamma\gamma \to Q\bar{Q}$ process in the k_{T}-factorization approach has the following form:

$$
\mathrm{d}\sigma_{1-\mathrm{res}}(\gamma\gamma \to Q\bar{Q})
$$
$$
= \int \frac{\mathrm{d}x}{x} \mathcal{A}_\gamma(x, \mathbf{k}_{\mathrm{T}}^2, \mu^2) \mathrm{d}\mathbf{k}_{\mathrm{T}}^2 \frac{\mathrm{d}\phi}{2\pi} \mathrm{d}\hat{\sigma}(\gamma g^* \to Q\bar{Q}), \quad (1)
$$

where $\hat{\sigma}(\gamma g^* \to Q\bar{Q})$ is the heavy quark production cross section via an off-shell gluon having a fraction x of the photon's longitudinal momentum, the non-zero transverse momentum $\mathbf{k}_{\mathrm{T}}$ ($\mathbf{k}_{\mathrm{T}}^2 = -k_{\mathrm{T}}^2 \neq 0$) and an azimuthal angle ϕ. The expression (1) can be easily rewritten as

$$
\frac{\mathrm{d}\sigma_{1-\mathrm{res}}(\gamma\gamma \to Q\bar{Q})}{\mathrm{d}y_2 \mathrm{d}\mathbf{p}_{2\mathrm{T}}^2}
$$
$$
= \int \frac{1}{16\pi(xs)^2(1-\alpha_2)} \mathcal{A}_\gamma(x, \mathbf{k}_{\mathrm{T}}^2, \mu^2)
$$
$$
\times |\bar{\mathcal{M}}|^2(\gamma g^* \to Q\bar{Q}) \mathrm{d}\mathbf{k}_{\mathrm{T}}^2 \frac{\mathrm{d}\phi}{2\pi} \frac{\mathrm{d}\phi_2}{2\pi}, \quad (2)
$$

where $|\bar{\mathcal{M}}|^2(\gamma g^* \to Q\bar{Q})$ is the off-shell matrix element, $s = (p_\gamma^{(1)} + p_\gamma^{(2)})^2$ is the total CM frame energy, y_2 and ϕ_2 are the rapidity and the azimuthal angle of the produced heavy quark having mass m_Q, $\alpha_2 = m_{2\mathrm{T}} \exp(y_2)/\sqrt{s}$ and $m_{2\mathrm{T}}^2 = m_Q^2 + \mathbf{p}_{2\mathrm{T}}^2$. To calculate the single-resolved contribution to the inclusive J/ψ production the same formula (2) can be used where the off-shell matrix element $|\bar{\mathcal{M}}|^2(\gamma g^* \to Q\bar{Q})$ should be replaced by one which corresponds to the $\gamma g^* \to J/\psi + g$ production process.

The available experimental data [1–5,35] refer to heavy quark or quarkonium production in the e^+e^- collisions also. In order to obtain these total cross sections, the $\gamma\gamma$ cross sections need to be weighted with the photon flux in the electron:

$$
\mathrm{d}\sigma(e^+e^- \to e^+e^- Q\bar{Q} + X) \quad (3)
$$
$$
= \int f_{\gamma/e}(x_1)\mathrm{d}x_1 \int f_{\gamma/e}(x_2)\mathrm{d}x_2\, \mathrm{d}\sigma(\gamma\gamma \to Q\bar{Q}),
$$

where we use the Weizäcker–Williams approximation for the bremsstrahlung photon distribution from an electron:

$$
f_{\gamma/e}(x) = \frac{\alpha}{2\pi} \left(\frac{1 + (1-x)^2}{x} \ln \frac{Q_{\max}^2}{Q_{\min}^2} \right.
$$

$$
\left. + 2m_e^2 x \left(\frac{1}{Q_{\max}^2} - \frac{1}{Q_{\min}^2} \right) \right), \quad (4)
$$

with $Q_{\min}^2 = m_e^2 x^2/(1-x)^2$ and $Q_{\max}^2 = Q_{\min}^2 + (E\theta)^2(1-x)$. Here $x = E_\gamma/E_e$, $E = E_e = \sqrt{s}/2$, s is the total energy in the e^+e^- collision, and $\theta \sim 30$ mrad is the angular cut that ensures that the photon is quasi-real.

The multidimensional integration in (2) and (3) has been performed by means of the Monte Carlo technique, using the routine VEGAS [37]. The full C++ code is available from the authors on request[2]. For the reader's convenience, we collect the analytic expressions for the off-shell matrix elements $|\mathcal{M}|^2(\gamma g^* \to Q\bar{Q})$ and $|\mathcal{M}|^2(\gamma g^* \to J/\psi g)$ in the appendix, including, in particular, the relevant formulas for the helicity zero J/ψ production state.

3 Numerical results

First of all, we can perform the integration of the unintegrated gluon distribution $\mathcal{A}_\gamma(x, k_{\mathrm{T}}^2, \mu^2)$ [25] over the gluon transverse momenta $\mathbf{k}_{\mathrm{T}}^2$ to obtain the effective gluon density in the photon:

$$
xg_\gamma(x, \mu^2) \sim \int_0^{\mu^2} \mathcal{A}_\gamma(x, \mathbf{k}_{\mathrm{T}}^2, \mu^2)\mathrm{d}\mathbf{k}_{\mathrm{T}}^2. \quad (5)
$$

The effective density $xg_\gamma(x, \mu^2)$ can be compared with the experimental data [38, 39] taken by the H1 collaboration at HERA. As seen in Figs. 1 and 2, this gluon distribution agrees well with the existing data extracted from hard dijet photoproduction (mean $p_{\mathrm{T}}^2 = 38\,\mathrm{GeV}^2$ [38] and $p_{\mathrm{T}}^2 = 74\,\mathrm{GeV}^2$ [39]). In contrast, the KMR construction of the unintegrated gluon density in the photon tends to underestimate the HERA data at $x < 10^{-1}$ [23].
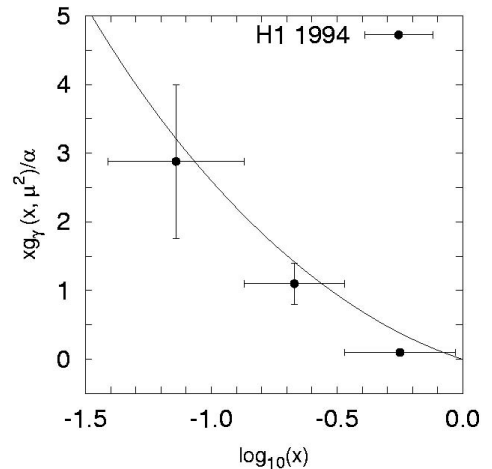
Fig. 1. The effective gluon distribution $xg_\gamma(x, \mu^2)$ in the photon as a function of $\log_{10}x$ at $\mu^2 = 38\,\mathrm{GeV}^2$. The experimental data [38] are from the H1 collaboration using hard dijets production
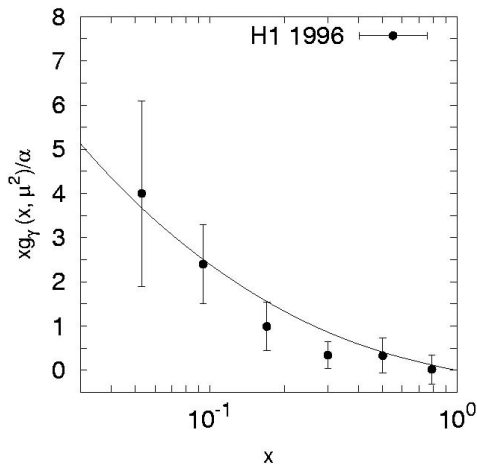
Fig. 2. The effective gluon distribution $xg_\gamma(x, \mu^2)$ in the photon as a function of x at $\mu^2 = 74 \, \text{GeV}^2$. The experimental data [38] are from the H1 collaboration using hard dijets production

Being sure that the full CCFM-evolved unintegrated gluon density $\mathcal{A}_\gamma(x, k_T^2, \mu^2)$ reproduces well the experimental data for $xg_\gamma(x, \mu^2)$, we are now in a position to present our numerical results. We describe first our theoretical input and the kinematical conditions. The cross sections for heavy quark and quarkonium production depend on the heavy quark mass and the energy scale μ^2. Since there are no free quarks due to the confinement effect, their masses cannot be measured directly and should be defined from hadron properties. In our analysis we have examined the following choice: $m_c = 1.4 \pm 0.1 \, \text{GeV}$ for the charm and $m_b = 4.75 \pm 0.25 \, \text{GeV}$ for the bottom quark masses. Such a variation of the quark masses gives the largest uncertainties in comparison with the scale variation[3] and therefore can be used as an estimate of the total theoretical uncertainties. Then, we will apply the standard expression $\mu^2 = m_Q^2 + \mathbf{p}_T^2$ for both renormalization and factorization scales. Here $\mathbf{p}_T$ is the transverse momentum of the heavy quark in the center-of-mass frame. We use the LO formula for the strong coupling constant $\alpha_s(\mu^2)$ with $n_f = 4$ active quark flavors and $\Lambda_{\text{QCD}} = 200 \, \text{MeV}$, such that $\alpha_s(M_Z^2) = 0.1232$. But $\Lambda_{\text{QCD}} = 340 \, \text{MeV}$ [7] was tested also.

Figure 3 confronts the total cross section $\sigma(\gamma\gamma \to c\bar{c} + X)$ calculated as a function of the photon–photon total energy $W_{\gamma\gamma}$ with the experimental data [2] taken by the L3 collaboration in the interval $5 < W_{\gamma\gamma} < 70 \, \text{GeV}$. The solid line represents the calculations with the charm mass $m_c = 1.4 \, \text{GeV}$, whereas the upper and lower dashed lines correspond to $m_c = 1.3 \, \text{GeV}$ and $m_c = 1.5 \, \text{GeV}$ respectively. It is clear that k_T-factorization reproduces well both the energy dependence and the normalization. One can see that the sensitivity of the results to the variations of the charm mass is rather large: shifting the mass down to $m_c = 1.3 \, \text{GeV}$ changes the estimated cross section by 15–20% at $W_{\gamma\gamma} \sim 60 \, \text{GeV}$. But in general all three curves lie within the experimental uncertainties.

---

[3] It was shown [25] that the Monte Carlo generator CASCADE [19,40] predicts very similar results for the total charm cross section with both scales $\mu^2 = m_Q^2 + \mathbf{p}_T^2$ and $\mu^2 = 4m_Q^2$.
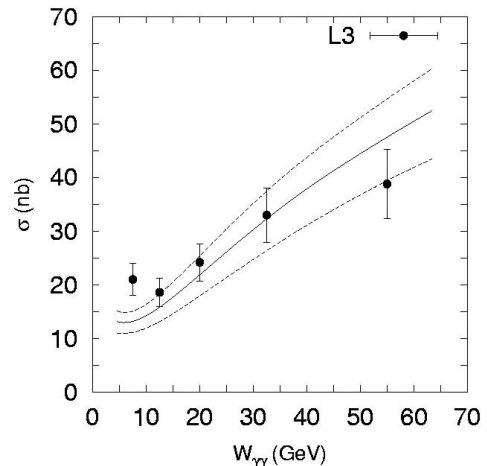

Fig. 3. The open charm total cross section $\sigma(\gamma\gamma \to c\bar{c} + X)$ as a function of $W_{\gamma\gamma}$ at $\sqrt{s} = 189$– $202 \, \text{GeV}$. The solid line corresponds to the charm mass $m_c = 1.4 \, \text{GeV}$, the upper and lower dashed lines correspond to the $m_c = 1.3 \, \text{GeV}$ and $m_c = 1.5 \, \text{GeV}$ respectively. The experimental data [2] are taken by the L3 collaboration
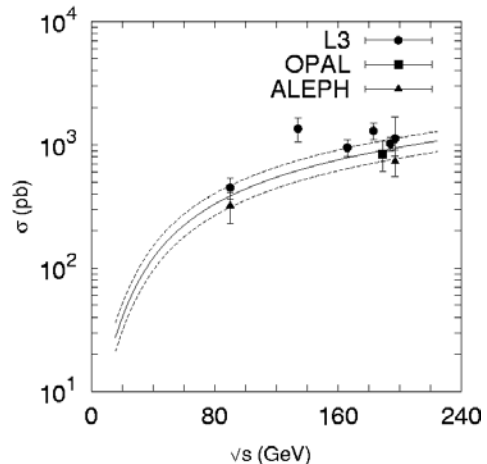
Fig. 4. The open charm total cross section $\sigma(e^+e^- \to e^+e^- c\bar{c} + X)$ as a function of the e^+e^- center-of-mass energy $\sqrt{s}$. All curves are the same as Fig. 3. The experimental data are from the L3 [1,3], OPAL [4] and ALEPH [5] collaborations

Experimental data for the total cross section $\sigma(e^+e^- \to e^+e^- c\bar{c} + X)$ come from the three LEP collaborations L3 [1,3], OPAL [4] and ALEPH [5]. In Fig. 4 we show our predictions in comparison with the data. All curves here are the same as in Fig. 3. One can see that our calculations describe the experimental data well again. The variation of the quark masses $1.3 < m_c < 1.5 \, \text{GeV}$ gives the theoretical uncertainties: approximately 15% in absolute normalization.

The available experimental data were obtained for the D^* meson production also. Two differential cross section are determined: first as a function of the transverse D^* momentum p_T, and second as a function of pseudo-rapidity $|\eta|$. In our calculation we convert the charmed quark into a D^* meson using the Peterson fragmentation function [41]. The default set for the fragmentation parameter ϵ_c and the fraction $f(c \to D^*)$ is $\epsilon_c = 0.06$ and $f(c \to D^*) = 0.26$. Other
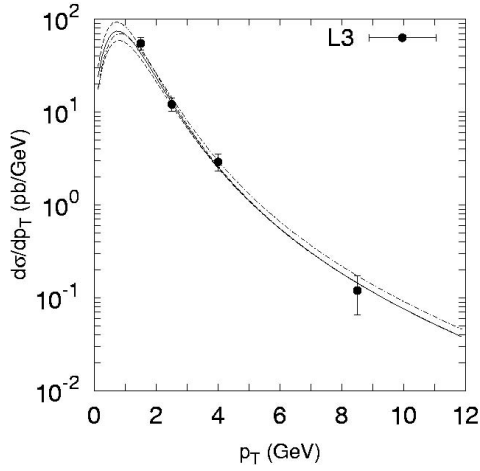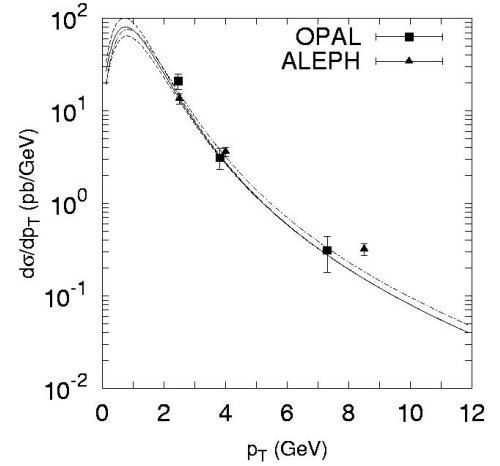
Fig. 5. The differential cross section $d\sigma/dp_T$ for inclusive D^* production at $|\eta| < 1.4$. The solid and both dashed curves here are the same as in Fig. 3 (calculated with the default value $\epsilon_c = 0.06$), dash-dotted curve represents results obtained using $\epsilon_c = 0.031$ and $m_c = 1.4\,\text{GeV}$. The experimental data are from L3 [3]

Fig. 6. The differential cross section $d\sigma/dp_T$ for inclusive D^* production at $|\eta| < 1.5$. All curves here are the same as in Fig. 5. The experimental data are from OPAL [4] and ALEPH [5]

Fig. 7. The differential D^* cross section $d\sigma/d|\eta|$ for the process $e^+e^- \rightarrow e^+e^- D^* + X$ in the $1 < p_T < 12\,\text{GeV}$ range. All curves here are the same as in Fig. 5. The experimental data are from L3 [3]

values for the parameter ϵ_c in the NLO perturbative QCD calculations are often used also, namely $\epsilon_c = 0.116$ [42] in the massless scheme and $\epsilon_c = 0.031$ [43] in the massive one. In the case of the massless calculation, this parameter was determined via a NLO fit to LEP1 data on D^* production in e^+e^- annihilation measured by the OPAL collaboration [44]. To investigate the sensitivity of our numerical results to the ϵ_c parameter, we have repeated our calculations using $\epsilon_c = 0.031$.

The recent L3 data [3] refer to the kinematic region defined by $1 < p_T < 12\,\text{GeV}$ and $|\eta| < 1.4$ with averaged total e^+e^- energy $\sqrt{s} = 193\,\text{GeV}$ ($183 < \sqrt{s} < 209\,\text{GeV}$). The OPAL data [4] were obtained in the region $2 < p_T < 12\,\text{GeV}$, $|\eta| < 1.5$ and averaged over $183 < \sqrt{s} < 189\,\text{GeV}$. The more recent ALEPH data [5] refer to the same kinematic region but averaged over $183 < \sqrt{s} < 209\,\text{GeV}$. We compare these three data sets with our calculation at $\sqrt{s} = 193\,\text{GeV}$. The different values of $\sqrt{s}$ are not expected to change the cross section more than the corresponding experimental errors. We have checked directly that shifting $\sqrt{s}$ from 189 to 193 GeV increases the calculated cross sections by about one percent only.

The transverse momenta distributions of the D^* meson for different pseudo-rapidity region in comparison to experimental data are shown in Figs. 5 and 6. The solid and both dashed curves here are the same as in Fig. 3 (calculated with the default value $\epsilon_c = 0.06$), dash-dotted curves represent results obtained using $\epsilon_c = 0.031$ and $m_c = 1.4\,\text{GeV}$. The overall agreement between the our predictions and the data is good although the ALEPH data points in the medium and large p_T range lie slightly above the theoretical curves. Shifting the ϵ_c default value down to $\epsilon_c = 0.031$ results in a slight broadening of the p_T spectra, which is insufficient to describe the data. The effects come from changing of the charm mass present only at low p_T: the predicted cross section $d\sigma/dp_T$ with $m_c = 1.3\,\text{GeV}$ is 10–15% above the one calculated with $m_c = 1.4\,\text{GeV}$ at $p_T \sim 1\,\text{GeV}$, whereas
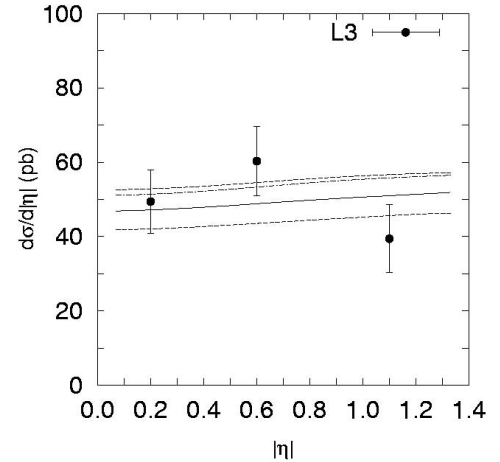
the solid and both dashed theoretical curves practically coincide at medium and large p_T. A similar effect was found in the NLO perturbative calculation [45], where the difference between the massive and massless approach arises at low p_T only.

The D^* pseudo-rapidity distributions compared with the experimental data in different p_T ranges are shown in Figs. 7 and 8. All curves here are the same as in Fig. 5. Our calculations agree well with the measured differential cross sections but slightly underestimate the OPAL data. However, setting $\epsilon_c = 0.031$ increases the absolute normalization of the pseudo-rapidity distribution by approximately 10%, and the agreement with the OPAL data becomes better. Again, one can see a significant mass dependence at low transverse momenta only: the difference between the theoretical curves calculated at $2 < p_T < 12\,\text{GeV}$ and plotted in Fig. 8 is much smaller than difference between the results presented in Fig. 7 obtained at $1 < p_T < 12\,\text{GeV}$.

We conclude from Figs. 3–8 that our calculations agree well with the charm data at LEP2. In contrast to the charm
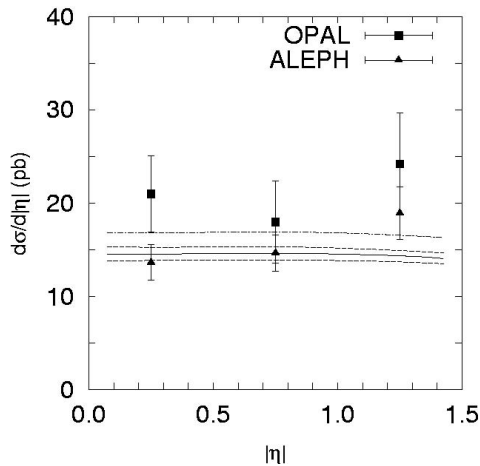
Fig. 8. The differential D^* cross section $d\sigma/d|\eta|$ for the process $e^+e^- \to e^+e^- D^* + X$ in the $2 < p_T < 12$ GeV range. All curves here are the same as in Fig. 5. The experimental data are from the OPAL [4] and ALEPH [5] collaborations
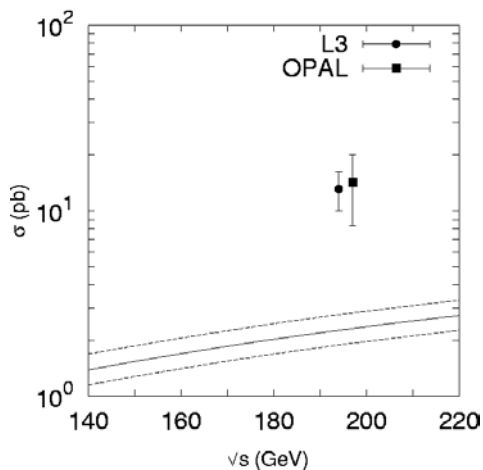
Fig. 9. The bottom total cross section $\sigma(e^+e^- \to e^+e^- b\bar{b} + X)$ as a function of the e^+e^- center-of-mass energy $\sqrt{s}$. The solid line corresponds to the bottom mass $m_b = 4.75$ GeV, the upper and lower dashed lines correspond to the $m_b = 4.5$ GeV and $m_b = 5.0$ GeV respectively. The experimental data are from the L3 [1] and OPAL [4]

case, the open bottom production in $\gamma\gamma$ collisions is clearly underestimated by k_T-factorization. Figure 9 shows our prediction for the open bottom cross section compared to the L3 [1] and OPAL [4] experimental data. Using the low but still reasonable b-quark mass $m_b = 4.5$ GeV, we obtain $\sigma(e^+e^- \to e^+e^- b\bar{b} + X) = 2.94$ pb at $\sqrt{s} = 200$ GeV. The very similar value $\sigma = 2.7$ pb was obtained [23] within the GBW saturation model adopted for the photon. The Monte Carlo generator CASCADE predicts $\sigma = 4.9$ pb [25] where a normalization factor $n = 1.7$ has been applied for the resolved contributions. The calculation [23] based on the KMR prescription for the unintegrated gluon density gives a lower cross section, $\sigma = 1.9$ pb. At the same time the prediction of the massive NLO perturbative QCD calculation [43] is 3.88 pb for $m_b = 4.5$ GeV and 2.34 pb for $m_b = 5.2$ GeV respectively. All these results are signifi-

cantly (about a factor 2 or 3) lower than the experimental data.

Such a disagreement between theory and data for bottom production at LEP2 is surprising and needs an explanation. It is known that a similar difference between theory and data was claimed for inclusive bottom hadroproduction at Tevatron. Recent analysis indicates that the overall description of these data can be improved [46] by adopting the non-perturbative fragmentation function of the b-quark into the B meson: an appropriate treatment of the b-quark fragmentation properties considerably reduces the disagreement between measured bottom cross section and the corresponding NLO calculations. It would be interesting to find out whether the similar explanation is also true for the L3 and OPAL experimental data.

After we have studied open heavy quark production at LEP2, we will investigate the production of heavy quarkonium in $\gamma\gamma$ interactions. As was already mentioned above, non-relativistic QCD gives a good description [36] of the recent DELPHI data [35] on inclusive J/ψ production at LEP2. We will examine whether the DELPHI data can be explained within the CS model using the k_T-factorization approach and CCFM-based unintegrated gluon density in the photon. Again, only direct and single-resolved contributions are taken into account.

Now we change the default set of parameters which were used in the case of open charm calculations. Since we neglect the relative momentum of the c-quarks (which form a J/ψ meson) the charm mass should be taken $m_c = m_\psi/2$. Therefore as the default choice in the following we will use $m_c = 1.55$ GeV. On the other hand there are many examples when a smaller value $m_c = 1.4$ GeV is used [30, 32, 36] in the calculation of J/ψ production. In our analysis we will apply this value as an extreme choice to investigate the theoretical uncertainties of the calculations.

The DELPHI data [35] refer to the kinematic region defined by $-2 < y_\psi < 2$ with the total e^+e^- energy $\sqrt{s} = 197$ GeV, where y_ψ is the J/ψ rapidity. However these data were obtained starting from very low transverse momenta, $p_{\psi T}^2 \sim 0.2$ GeV^2. We note that the k_T-factorization as well as the usual collinear factorization theorem does not work well for such $p_{\psi T}$ values, and our calculations should be compared with the experimental data at approximately $p_{\psi T} > 1$ GeV only. In Fig. 10 we confront our theoretical predictions with the measured differential cross section $d\sigma/dp_{\psi T}^2$. The solid line corresponds to the default set of parameters and lies below the data by a factor of about 2 or 3. This discrepancy is not dramatic, because some reasonable variations in m_c and Λ_{QCD}, namely $200 < \Lambda_{QCD} < 340$ MeV and $1.4 < m_c < 1.55$ GeV, change the estimated cross section by a factor of 3 (dashed line in Fig. 9). Thus the visible disagreement is removed. However, we do not interpret this as a strong indication of consistency between data and theory, but rather as a consequence of a wide uncertainty band. Better future experimental studies are crucial to determine whether the results of our calculations contradict the DELPHI data points.

The main difference between k_T-factorization and other approaches is connected with the polarization properties of the final particles because the initial off-shell gluons do
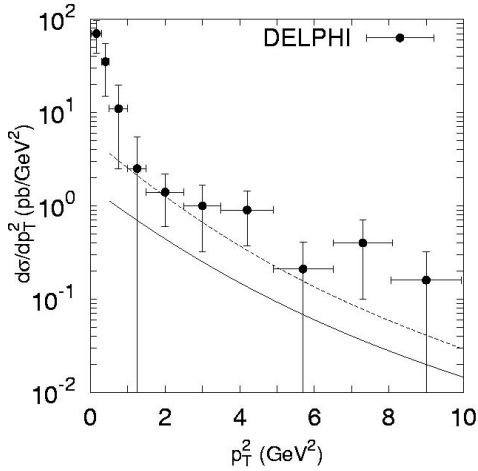
Fig. 10. The cross section $d\sigma/dp^2_{\psi\rm T}$ of $e^+e^- \to e^+e^- J/\psi + X$ measured by the DELPHI collaboration [35] at $2 < y_\psi < 2$ as a function of $p^2_{\psi\rm T}$ is compared with the $k_{\rm T}$-factorization calculations in the CS model. The solid line corresponds to the $m_c = 1.55\,{\rm GeV}$ and $\Lambda_{\rm QCD} = 200\,{\rm MeV}$, the dashed line corresponds to the $m_c = 1.4\,{\rm GeV}$ and $\Lambda_{\rm QCD} = 340\,{\rm MeV}$

Fig. 11. The $p^2_{\psi\rm T}$-dependence of the spin alignment parameter α for the inclusive J/ψ production. The solid line corresponds to the $k_{\rm T}$-factorization predictions, the dashed line corresponds to the collinear leading order pQCD calculations with the GRV (LO) gluon density in a photon
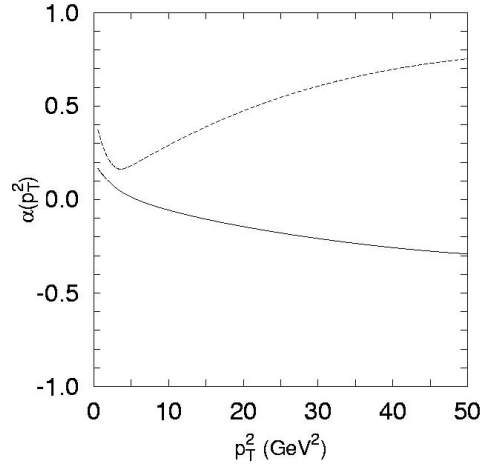
directly influence the J/ψ spin alignment [32–34]. Only a very small fraction of J/ψ mesons can be produced in the helicity zero state (longitudinal polarization) by massless bosons. This property is totally determined by the subprocess matrix element structure. The degree of spin alignment can be measured experimentally since the different polarization states of the J/ψ meson result in significantly different angular distributions of the $J/\psi \to \mu^+\mu^-$ decay leptons:

$$\frac{d\Gamma(J/\psi \to \mu^+\mu^-)}{d\cos\theta} \sim 1 + \alpha\cos^2\theta, \qquad (6)$$

where $\alpha = 1$ for transverse and $\alpha = -1$ for longitudinal polarizations, respectively. Here θ is the angle between the lepton and J/ψ directions, measured in the J/ψ meson rest frame. We calculate the $p^2_{\rm T}$-dependence of the spin alignment parameter as

$$\alpha(p^2_{\psi\rm T}) = \frac{1 - 3\xi(p^2_{\psi\rm T})}{1 + \xi(p^2_{\psi\rm T})}, \qquad (7)$$

with $\xi(p^2_{\psi\rm T})$ being the fraction of longitudinally polarized J/ψ mesons. The results of our calculations are shown in Fig. 11. The solid line represents the $k_{\rm T}$-factorization predictions and the dashed line corresponds to the collinear leading-order pQCD ones with the GRV (LO) gluon density [47] of the photon. One can see that the fraction of longitudinally polarized mesons increases with $p^2_{\psi\rm T}$ within the $k_{\rm T}$-factorization approach. This fact is in clear contradiction with the usual collinear parton model result. The $k_{\rm T}$-factorization calculations made for the inelastic J/ψ production at HERA [32,34] and Tevatron [33] show the same behavior of the α parameter, whereas the collinear parton model and NRQCD predict a strong transverse polarization at moderate and large $p^2_{\psi\rm T}$ range. We point out that our predictions for the J/ψ polarization are stable

with respect to variation of the model parameters, such as charm quark mass and factorization scale. In fact, there is no dependence on the strong coupling constant which cancels out. At the same time the DELPHI fit [35] gives $\alpha = 0.7 \pm 1.3$ for $p^2_{\psi\rm T} > 1\,{\rm GeV}^2$, which has, however, huge experimental uncertainties. Since the account of the octet contributions does not change the predictions of the $k_{\rm T}$-factorization approach for the spin alignment parameter α [33], the future extensive experimental study of such processes will be a direct probe of the gluon virtuality.

4 Conclusions

We have investigated heavy flavor production in photon–photon interactions at high energies within the framework of $k_{\rm T}$-factorization, using the unintegrated gluon distribution obtained from the full CCFM evolution equation for the photon. We have calculated total and differential cross sections of open charm and bottom production including D^* meson transverse momenta and pseudo-rapidity distributions. Also we have studied inclusive J/ψ production at LEP2 using a color-singlet model supplemented with $k_{\rm T}$-factorization.

We take into account both the direct and single-resolved contribution and investigate the sensitivity of the our results to different parameters, such as heavy quark mass, charm fragmentation and the $\Lambda_{\rm QCD}$ parameter. There are, of course, also some uncertainties due to the renormalization and factorization scales. However, these effects would not be large enough to change the conclusions presented here and were not taken into account in our analysis.

The results of calculations with the default parameter set agree well with open charm production data taken by the L3, OPAL and ALEPH collaborations at LEP2. In contrast, the bottom production cross section is clearly underestimated by a factor about 3. A potential explanation of this fact may be, perhaps, connected with the more

accurate treatment of the b-quark fragmentation function. Our prediction for the inclusive J/ψ production slightly underestimate the DELPHI data. However, a strong inconsistency cannot be claimed, because of the large experimental errors and theoretical uncertainties. Therefore more precise future experiments, especially polarized quarkonium production, are necessary to decide whether our predictions contradict the experimental data.

In conclusion, we point out that at the CERN LEP2 collider (as well as at HERA and Tevatron) the difference between predictions of the collinear and k_{T}-factorization approaches is clearly visible in polarized heavy quarkonium production. It comes directly from initial gluon off-shellness. The experimental study of such processes should be an additional test of non-collinear parton evolution.

Appendix

Here we present the compact analytic expressions for the off-shell matrix elements which appear in (2). In the following, $\hat{s}$, $\hat{t}$, $\hat{u}$ are the usual Mandelstam variables for the $2 \to 2$ process and e_Q is the fractional electric charge of the heavy quark Q.

We start from the photon–gluon fusion $\gamma(q)g^*(k) \to Q(p_1)\bar{Q}(p_2)$ subprocess, where the initial off-shell gluon has non-zero virtuality $\mathbf{k}_{\mathrm{T}}^2$. The corresponding squared matrix element summed over the final polarization states and averaged over the initial ones reads

$$|\bar{\mathcal{M}}|^2(\gamma g^* \to Q\bar{Q}) = -\frac{(4\pi)^2 e_Q^2 \alpha \alpha_{\mathrm{s}}}{(\hat{t} - m^2)^2(\hat{u} - m^2)^2} F_{Q\bar{Q}}(\mathbf{k}_{\mathrm{T}}^2),$$

$$(A.1)$$

where m is the heavy quark mass, and

$$F_{Q\bar{Q}}(\mathbf{k}_{\mathrm{T}}^2)$$
$$= 6m^8 - (2\mathbf{k}_{\mathrm{T}}^4 + 2(\hat{t} + \hat{u})\mathbf{k}_{\mathrm{T}}^2 + 3\hat{t}^2 + 3\hat{u}^2 + 14\hat{t}\hat{u})m^4$$
$$+ (2(\hat{t} + \hat{u})\mathbf{k}_{\mathrm{T}}^4 + 8\hat{t}\hat{u}\mathbf{k}_{\mathrm{T}}^2 + \hat{t}^3 + \hat{u}^3 + 7\hat{t}\hat{u}^2 + 7\hat{t}^2\hat{u})m^2$$
$$- \hat{t}\hat{u}(2\mathbf{k}_{\mathrm{T}}^4 + 2(\hat{t} + \hat{u})\mathbf{k}_{\mathrm{T}}^2 + \hat{t}^2 + \hat{u}^2). \qquad (A.2)$$

We note that the matrix element of the direct contribution $\gamma\gamma \to Q\bar{Q}$ may be easily obtained from (A.1) and (A.2) in the limit $\mathbf{k}_{\mathrm{T}}^2 \to 0$, if we replace the normalization factor $(4\pi)^2 e_Q^2 \alpha \alpha_{\mathrm{s}}$ by $(4\pi)^2 \alpha^2 e_Q^4 N_c$ (where N_c is the number of colors) and average (A.2) over the transverse momentum vector $\mathbf{k}_{\mathrm{T}}$.

Now we are in a position to present our formulas for the $\gamma(q)g^*(k) \to J/\psi(p_\psi)g(p_g)$ subprocess. In the color-singlet model the production of the J/ψ meson is considered as a production of a quark–antiquark system in the color-singlet state with orbital momentum $L = 0$ and spin momentum $S = 1$. The squared off-mass shell matrix element summed over the final polarization states and averaged over the initial ones can be written as

$$|\bar{\mathcal{M}}|^2(\gamma g^* \to J/\psi g)$$

$$= -\frac{64 e_Q^2 (4\pi)^3 \alpha \alpha_{\mathrm{s}}^2 |\psi(0)|^2}{3 m_\psi (\hat{t} - m_\psi^2)^2 (\hat{u} - m_\psi^2 - \mathbf{k}_{\mathrm{T}}^2)^2 (\hat{t} + \hat{u} + \mathbf{k}_{\mathrm{T}}^2)^2 \mathbf{k}_{\mathrm{T}}^2}$$

$$\times F_\psi(\mathbf{k}_{\mathrm{T}}^2), \qquad (A.3)$$

where $|\psi(0)|^2 = 0.0876\,\mathrm{GeV}^3$ is the J/ψ wave function at the origin, m_ψ is the J/ψ meson mass, $\mathbf{k}_{\mathrm{T}}^2$ is the virtuality of the initial gluon, and the function $F_\psi(\mathbf{k}_{\mathrm{T}}^2)$ is given by

$$F_\psi(\mathbf{k}_{\mathrm{T}}^2) = \mathbf{k}_{\mathrm{T}}^2 \left(\mathbf{k}_{\mathrm{T}}^6 (m_\psi^2 - \hat{t})(m_\psi^2 - \hat{t} - \hat{u}) \right.$$
$$- m_\psi^2 \left(\hat{t}^2 + \hat{t}\hat{u} + \hat{u}^2 - m_\psi^2(\hat{t} + \hat{u}) \right)^2$$
$$+ \mathbf{k}_{\mathrm{T}}^4 \left(3m_\psi^6 + \hat{t}\hat{u}(\hat{t} + \hat{u}) - 3m_\psi^4(2\hat{t} + \hat{u}) \right.$$
$$\left. + m_\psi^2(3\hat{t}^2 + 2\hat{t}\hat{u} - \hat{u}^2) \right)$$
$$+ \mathbf{k}_{\mathrm{T}}^2 \left(2m_\psi^8 + m_\psi^4\hat{t}(\hat{t} - \hat{u}) - \hat{t}^2(\hat{t} + \hat{u})^2 \right.$$
$$\left. - 2m_\psi^6(2\hat{t} + \hat{u}) + m_\psi^2\hat{t}(2\hat{t}^2 + 5\hat{t}\hat{u} + 5\hat{u}^2)) \right)$$
$$+ 2\mathbf{k}_{\mathrm{T}}^2 \left(\mathbf{k}_{\mathrm{T}}^4(m_\psi^2 - \hat{t})(m_\psi^2 - \hat{t} - u) \right.$$
$$+ \mathbf{k}_{\mathrm{T}}^2 \left(3m_\psi^6 + \hat{t}(\hat{t} + \hat{u})^2 - m_\psi^4(5\hat{t} + 3\hat{u}) \right.$$
$$\left. + m_\psi^2(\hat{t}^2 + \hat{t}\hat{u} - 2\hat{u}^2) \right)$$
$$\left. + m_\psi^2 \left(2m_\psi^6 - m_\psi^4(3\hat{t} + 2\hat{u}) + \hat{t}(\hat{t}^2 + 2\hat{t}\hat{u} + 3\hat{u}^2)) \right) \right)$$
$$\times (-|\mathbf{p}_{\psi\mathrm{T}}||\mathbf{k}_{\mathrm{T}}| \cos\phi_2)$$
$$+ 2m_\psi^2 \left(m_\psi^2(-m_\psi^2 + \hat{t} + \hat{u})^2 \right.$$
$$\left. + \mathbf{k}_{\mathrm{T}}^2 (m_\psi^4 + \hat{t}^2 + 2\hat{t}\hat{u} - \hat{u}^2 - 2m_\psi^2(\hat{t} + \hat{u})) \right)$$
$$\times \mathbf{p}_{\psi\mathrm{T}}^2 \mathbf{k}_{\mathrm{T}}^2 \cos^2\phi_2. \qquad (A.4)$$

Here $\mathbf{p}_{\psi\mathrm{T}}$ is the J/ψ transverse momentum, and ϕ_2 is the azimuthal angle of the incoming virtual gluon having virtuality $\mathbf{k}_{\mathrm{T}}^2$. To study polarized J/ψ production we introduce the four-vector of the longitudinal polarization $\epsilon_{\psi,\mathrm{L}}^\mu$. In the frame where the z axis is oriented along the quarkonium momentum vector, $p_\psi^\mu = (E_\psi, 0, 0, |\mathbf{p}_\psi|)$, this polarization vector is $\epsilon_{\psi,L}^\mu = (|\mathbf{p}_\psi|, 0, 0, E_\psi)/m_\psi$. The squared off-shell matrix element reads

$$|\bar{\mathcal{M}}|_L^2(\gamma g^* \to J/\psi g)$$

$$= \frac{32 e_Q^2 (4\pi)^3 \alpha \alpha_{\mathrm{s}}^2 |\psi(0)|^2 m_\psi}{3(\hat{t} - m_\psi^2)^2 (\hat{u} - m_\psi^2 - \mathbf{k}_{\mathrm{T}}^2)^2 (\hat{t} + \hat{u} + \mathbf{k}_{\mathrm{T}}^2)^2 \mathbf{k}_{\mathrm{T}}^2} F_{\psi,L}(\mathbf{k}_{\mathrm{T}}^2),$$

where the function $F_{\psi,L}(\mathbf{k}_{\mathrm{T}}^2)$ is defined as

$$F_{\psi,L}(\mathbf{k}_{\mathrm{T}}^2) = -4\Delta_2\Delta_3 \mathbf{k}_{\mathrm{T}}^4 m_\psi^4 + 2\Delta_3^2 \mathbf{k}_{\mathrm{T}}^4 m_\psi^4 - 4\Delta_2\Delta_3 \mathbf{k}_{\mathrm{T}}^2 m_\psi^6$$

$+8\Delta_2\Delta_3\mathbf{k}_{\mathrm{T}}^4 m_\psi^2\hat{t} - 4\Delta_3^2\mathbf{k}_{\mathrm{T}}^4 m_\psi^2\hat{t} + 8\Delta_2\Delta_3\mathbf{k}_{\mathrm{T}}^2 m_\psi^4\hat{t}$

$+4\Delta_3^2\mathbf{k}_{\mathrm{T}}^2 m_\psi^4\hat{t} - 4\Delta_2\Delta_3\mathbf{k}_{\mathrm{T}}^4\hat{t}^2 + 2\Delta_3^2\mathbf{k}_{\mathrm{T}}^4\hat{t}^2 - 4\Delta_2\Delta_3\mathbf{k}_{\mathrm{T}}^2 m_\psi^2\hat{t}^2$

$-8\Delta_3^2\mathbf{k}_{\mathrm{T}}^2 m_\psi^2\hat{t}^2 + 2\Delta_3^2 m_\psi^4\hat{t}^2 + 4\Delta_3^2\mathbf{k}_{\mathrm{T}}^2\hat{t}^3 - 4\Delta_3^2 m_\psi^2\hat{t}^3$

$+2\Delta_3^2\hat{t}^4 + 4\Delta_2^2\mathbf{k}_{\mathrm{T}}^4 m_\psi^2\hat{u} - 4\Delta_2\Delta_3\mathbf{k}_{\mathrm{T}}^4 m_\psi^2\hat{u} + 2\Delta_3^2\mathbf{k}_{\mathrm{T}}^4 m_\psi^2\hat{u}$

$+4\Delta_2^2\mathbf{k}_{\mathrm{T}}^2 m_\psi^4\hat{u} + 2\Delta_3^2\mathbf{k}_{\mathrm{T}}^2 m_\psi^4\hat{u} - 4\Delta_2^2\mathbf{k}_{\mathrm{T}}^4\hat{t}\hat{u} + 4\Delta_2\Delta_3\mathbf{k}_{\mathrm{T}}^4\hat{t}\hat{u}$

$-2\Delta_3^2\mathbf{k}_{\mathrm{T}}^4\hat{t}\hat{u} - 4\Delta_2^2\mathbf{k}_{\mathrm{T}}^2 m_\psi^2\hat{t}\hat{u} - 4\Delta_2\Delta_3\mathbf{k}_{\mathrm{T}}^2 m_\psi^2\hat{t}\hat{u}$

$-4\Delta_3^2\mathbf{k}_{\mathrm{T}}^2 m_\psi^2\hat{t}\hat{u} + 2\Delta_3^2 m_\psi^4\hat{t}\hat{u} + 4\Delta_2\Delta_3\mathbf{k}_{\mathrm{T}}^2\hat{t}^2\hat{u} + 2\Delta_3^2\mathbf{k}_{\mathrm{T}}^2\hat{t}^2\hat{u}$

$-6\Delta_3^2 m_\psi^2\hat{t}^2\hat{u} + 4\Delta_3^2\hat{t}^3\hat{u} + \mathbf{k}_{\mathrm{T}}^6\hat{u}^2 - 4\Delta_2^2\mathbf{k}_{\mathrm{T}}^2 m_\psi^2\hat{u}^2$

$+4\Delta_2\Delta_3\mathbf{k}_{\mathrm{T}}^2 m_\psi^2\hat{u}^2 - 2\Delta_3^2\mathbf{k}_{\mathrm{T}}^2 m_\psi^2\hat{u}^2 + \mathbf{k}_{\mathrm{T}}^2 m_\psi^4\hat{u}^2$

$+4\Delta_2\Delta_3\mathbf{k}_{\mathrm{T}}^2\hat{t}\hat{u}^2 - 2\Delta_3^2\mathbf{k}_{\mathrm{T}}^2\hat{t}\hat{u}^2 - 2\mathbf{k}_{\mathrm{T}}^4\hat{t}\hat{u}^2 - 2\Delta_3^2 m_\psi^2\hat{t}\hat{u}^2$

$-2\mathbf{k}_{\mathrm{T}}^2 m_\psi^2\hat{t}\hat{u}^2 + 2\Delta_3^2\hat{t}^2\hat{u}^2 + 2\mathbf{k}_{\mathrm{T}}^2\hat{t}^2\hat{u}^2$

$-2\mathbf{k}_{\mathrm{T}}^2 m_\psi^2\hat{u}^3 + 2\mathbf{k}_{\mathrm{T}}^2\hat{t}\hat{u}^3 + \mathbf{k}_{\mathrm{T}}^2\hat{u}^4 + 8\Delta_1^2\mathbf{k}_{\mathrm{T}}^4(-m_\psi^2 + \hat{t} + \hat{u})^2$

$+4\Delta_1\mathbf{k}_{\mathrm{T}}^2\left(\Delta_2\left(\mathbf{k}_{\mathrm{T}}^4(2m_\psi^2 - 2\hat{t} - \hat{u}) + m_\psi^2(m_\psi^2 - 2\hat{t} - \hat{u})\hat{u}\right.\right.$

$+\mathbf{k}_{\mathrm{T}}^2\left(2m_\psi^4 + \hat{u}^2 - 2m_\psi^2(\hat{t} + \hat{u})\right)\right)$

$+\Delta_3\left(-m_\psi^6 + \mathbf{k}_{\mathrm{T}}^4(-m_\psi^2 + \hat{t})\right.$

$+2\hat{t}(\hat{t} + \hat{u})^2 + m_\psi^4(3\hat{t} + \hat{u}) - m_\psi^2\hat{t}(4\hat{t} + 3\hat{u})$

$+\mathbf{k}_{\mathrm{T}}^2\left(-\left(m_\psi^2(2\hat{t} + \hat{u})\right) + \hat{t}(2\hat{t} + 3\hat{u})\right)\right)$

$+4\left(-\left(\Delta_2\Delta_3(\mathbf{k}_{\mathrm{T}}^2 + m_\psi^2)(m_\psi^2 - \hat{t})(m_\psi^2 - \hat{t} - \hat{u})\right)\right.$

$+\mathbf{k}_{\mathrm{T}}^2(\mathbf{k}_{\mathrm{T}}^2 - \hat{t})\hat{u}^2 + 4\Delta_1^2\mathbf{k}_{\mathrm{T}}^2(-m_\psi^2 + \hat{t} + \hat{u})^2$

$+\Delta_1\left(2\Delta_2\mathbf{k}_{\mathrm{T}}^2\left(2m_\psi^4 + \mathbf{k}_{\mathrm{T}}^2(2m_\psi^2 - 2\hat{t} - \hat{u})\right.\right.$

$-2m_\psi^2(\hat{t} + \hat{u}) + \hat{u}(\hat{t} + \hat{u}))$

$-\Delta_3\left(m_\psi^6 + \mathbf{k}_{\mathrm{T}}^4(m_\psi^2 - \hat{t} + \hat{u})\right.$

$-2\hat{t}(\hat{t} + \hat{u})^2 - m_\psi^4(3\hat{t} + 2\hat{u}) + m_\psi^2(4\hat{t}^2 + 5\hat{t}\hat{u} + \hat{u}^2)$

$+\mathbf{k}_{\mathrm{T}}^2\left(-2\hat{t}^2 - t\hat{u} + \hat{u}^2 + m_\psi^2(2\hat{t} + \hat{u})\right))))$

$\times(-|\mathbf{p}_{\psi\mathrm{T}}||\mathbf{k}_{\mathrm{T}}|\cos\phi_2)$

$+4(2\Delta_1\Delta_2(\mathbf{k}_{\mathrm{T}}^2 + m_\psi^2)(m_\psi^2 - \hat{t} - \hat{u})$

$+\mathbf{k}_{\mathrm{T}}^2\hat{u}^2 + 2\Delta_1^2(-m_\psi^2 + \hat{t} + \hat{u})^2)\mathbf{p}_{\psi\mathrm{T}}^2\mathbf{k}_{\mathrm{T}}^2\cos^2\phi_2, \qquad (\mathrm{A.5})$

and the following notation has been used:

$$\Delta_1 = (\alpha_1 + \alpha_2)\frac{\sqrt{s}}{2m_\psi}$$

$$\times\left(\sqrt{\mathbf{p}_{\psi\mathrm{T}}^2 + s(\alpha_1 - \beta_1)^2/4}\right.$$

$$\left. - \frac{s(\alpha_1^2 - \beta_1^2)}{4\sqrt{\mathbf{p}_{\psi\mathrm{T}}^2 + s(\alpha_1 - \beta_1)^2/4}}\right),$$

$$\Delta_2 = (\beta_1 + \beta_2)\frac{\sqrt{s}}{2m_\psi}$$

$$\times\left(\sqrt{\mathbf{p}_{\psi\mathrm{T}}^2 + s(\alpha_1 - \beta_1)^2/4}\right.$$

$$\left. + \frac{s(\alpha_1^2 - \beta_1^2)}{4\sqrt{\mathbf{p}_{\psi\mathrm{T}}^2 + s(\alpha_1 - \beta_1)^2/4}}\right) + \Delta_3,$$

$$\Delta_3 = -\frac{\sqrt{s}(\alpha_1 + \beta_1)}{2m_\psi\sqrt{\mathbf{p}_{\psi\mathrm{T}}^2 + s(\alpha_1 - \beta_1)^2/4}}|\mathbf{p}_{\psi\mathrm{T}}||\mathbf{k}_{\mathrm{T}}|\cos\phi_2,$$

$$\alpha_1 = \sqrt{\frac{m_\psi^2 + \mathbf{p}_{\psi\mathrm{T}}^2}{s}}\exp(y_\psi),$$

$$\beta_1 = \sqrt{\frac{m_\psi^2 + \mathbf{p}_{\psi\mathrm{T}}^2}{s}}\exp(-y_\psi),$$

$$\alpha_2 = \frac{|\mathbf{p}_{g\mathrm{T}}|}{\sqrt{s}}\exp(y_g), \quad \beta_2 = \frac{|\mathbf{p}_{g\mathrm{T}}|}{\sqrt{s}}\exp(-y_g). \qquad (\mathrm{A.6})$$

References

1. M. Acciari et al. (L3 Collaboration), Phys. Lett. B **503**, 10 (2001)
2. M. Acciari et al. (L3 Collaboration), Phys. Lett. B **514**, 19 (2001)
3. P. Achard et al. (L3 Collaboration), Phys. Lett. B **535**, 59 (2002)
4. G. Abbiendi et al. (OPAL Collaboration), Eur. Phys. J. C **16**, 579 (2000)
5. ALEPH Collaboration, Eur. Phys. J. C **28**, 437 (2003)
6. TESLA Technical Design Report, DESY 2001-11, TESLA Report 2001-23, TESLA-FEL 2001-05
7. M. Drees, M. Krämer, J. Zunft, P.M. Zerwas, Phys. Lett. B **306**, 371 (1993)
8. V.N. Gribov, L.N. Lipatov, Yad. Fiz. **15**, 781 (1972); L.N. Lipatov, Sov. J. Nucl. Phys. **20**, 94 (1975); G. Altarelli, G. Parisi, Nucl. Phys. B **126**, 298 (1977); Y.L. Dokshitzer, Sov. Phys. JETP **46**, 641 (1977)
9. V.N. Gribov, E.M. Levin, M.G. Ryskin, Phys. Rep. **100**, 1 (1983)
10. E.M. Levin, M.G. Ryskin, Yu.M. Shabelsky, A.G. Shuvaev, Sov. J. Nucl. Phys. **53**, 657 (1991)
11. S. Catani, M. Ciafaloni, F. Hautmann, Nucl. Phys. B **366**, 135 (1991)
12. J.C. Collins, R.K. Ellis, Nucl. Phys. B **360**, 3 (1991)
13. E.A. Kuraev, L.N. Lipatov, V.S. Fadin, Sov. Phys. JETP **44**, 443 (1976); **45**, 199 (1977); I.I. Balitsky, L.N. Lipatov, Sov. J. Nucl. Phys. **28**, 822 (1978)
14. B. Andersson et al. (Small-x Collaboration), Eur. Phys. J. C **25**, 77 (2002)
15. M. Ciafaloni, Nucl. Phys. B **296**, 49 (1988); S. Catani, F. Fiorani, G. Marchesini, Phys. Lett. B **234**, 339 (1990); Nucl. Phys. B **336**, 18 (1990); G. Marchesini, Nucl. Phys. B **445**, 49 (1995)
16. J.R. Forshaw, A. Sabio Vera, Phys. Lett. B **440**, 141 (1998)
17. B.R. Webber, Phys. Lett. B **444**, 81 (1998)
18. G.P. Salam, JHEP **03**, 009 (1999)
19. H. Jung, G.P. Salam, Eur. Phys. J. C **19**, 351 (2001)
20. M.A. Kimber, A.D. Martin, M.G. Ryskin, Phys. Rev. D **63**, 114027 (2001)

21. J. Kwiecinski, Acta Phys. Polon. B **33**, 1809 (2002)
22. A. Gawron, J. Kwiecinski, Acta Phys. Polon. B **34**, 133 (2003)
23. L. Motyka, N. Timneanu, Eur. Phys. J. C **27**, 73 (2003)
24. K. Golec-Biernat, M. Wüsthoff, Phys. Rev. D **59**, 014017 (1999); D **60**, 114023 (1999)
25. M. Hansson, H. Jung, L. Jönsson, hep-ph/0402019
26. A.V. Lipatov, N.P. Zotov, hep-ph/0304181
27. J. Blümlein, DESY 95-121; DESY 95-125
28. G.T. Bodwin, E. Braaten, G.P. Lepage, Phys. Rev. D **51**, 1125 (1995); D **55**, 5853 (1997)
29. E. Braaten, S. Fleming, Phys. Rev. Lett. **74**, 3327 (1995); E. Braaten, T.C. Yuan, Phys. Rev. D **52**, 6627 (1995); P. Cho, A.K. Leibovich, Phys. Rev. D **53**, 150 (1996); D **53**, 6203 (1996)
30. M. Cacciari, M. Kramër, Phys. Rev. Lett. **76**, 4128 (1996); P. Ko, J. Lee, H.-S. Song, Phys. Rev. D **54**, 4312 (1996); M. Beneke, M. Kramër, M. Vänttinen, Phys. Rev. D **57**, 4258 (1998)
31. M. Beneke, M. Kramër, Phys. Rev. **55**, 5269 (1997); A.K. Leibovich, Phys. Rev. D **56**, 4412 (1997); E. Braaten, B.A. Kniehl, J. Lee, Phys. Rev. D **62**, 094005 (2000)
32. A.V. Lipatov, N.P. Zotov, Eur. Phys. J. C **27**, 87 (2003); Yad. Fiz. **67**, 846 (2004)
33. S.P. Baranov, Phys. Rev. D **66**, 114003 (2002)
34. S.P. Baranov, Phys. Lett. B **428**, 377 (1998); S.P. Baranov, N.P. Zotov, J. Phys. G **29**, 1395 (2003)
35. J. Abdallah et al. (DELPHI Collaboration), Phys. Lett. B **565**, 76 (2003)
36. M. Klasen, B.A. Kniehl, L.N. Mihaila, M. Steinhauser, Phys. Rev. Lett. **89**, 032001 (2002)
37. G.P. Lepage, J. Comput. Phys. **27**, 192 (1978)
38. C. Adloff et al. (H1 Collaboration), Eur. Phys. J. C **10**, 363 (1999)
39. C. Adloff et al. (H1 Collaboration), Phys. Lett. B **483**, 36 (2000)
40. H. Jung, Comput. Phys. Comm. **143**, 100 (2002)
41. C. Peterson, D. Schlatter, I. Schmitt, P. Zervas, Phys. Rev. D **27**, 105 (1983)
42. S. Frixione, M. Krämer, E. Laenen, Nucl. Phys. B **571**, 169 (2000)
43. J. Binnewies, B.A. Kniehl, G. Krämer, Phys. Rev. D **53**, 6110 (1996); D **58**, 014014 (1998)
44. K. Ackerstaff et al. (OPAL Collaboration), Eur. Phys. J. C **1**, 439 (1998)
45. G. Krämer, H. Spiesberger, Eur. Phys. J. C **22**, 289 (2001)
46. M. Cacciari, P. Nason, Phys. Rev. Lett. **89**, 122003 (2002); M. Cacciari, S. Frixione, M.L. Mangano, P. Nason, G. Ridolfi, JHEP **0407**, 033 (2004)
47. M. Glück, E. Reya, A. Vogt, Z. Phys. C **67**, 433 (1995)